Influence of the Carbon Nanotube Probe Tilt Angle on the Effective Probe Stiffness and Image Quality in Tapping-Mode Atomic Force Microscopy

Santiago D. Solares, Yuki Matsuda, and William A. Goddard III*

Materials and Process Simulation Center, Division of Chemistry and Chemical Engineering, California Institute of Technology, Pasadena, California 91125

Received: May 25, 2005; In Final Form: July 11, 2005

Previous studies have shown that when using carbon nanotubes (CNTs) as tapping-mode AFM probes, their tilt angle with respect to vertical (denoted ϕ) must be close to 0° to obtain high-quality images and that very poor images are obtained for $\phi > 30°$. Here we present a *quantitative* theoretical investigation of the effect of ϕ on tapping-mode AFM imaging for single-wall and multiwall nanotube (SWNT and MWNT, respectively) probes of diameters 3.4−5.5 nm and aspect ratio 7.5, which have been found ideal for imaging via TEM. Using molecular and classical dynamics, we investigate the effect of ϕ on CNT probe stiffness (quantified through the maximum gradient of the tip−sample interaction force) and show that it decreases linearly with increasing ϕ, becoming negligible at around $\phi \approx 40°$, thus confirming the conclusions of previous studies. We find that MWNT probe stiffness is proportional to the number of walls, but that the difference in stiffness between SWNTs and MWNTs also decreases linearly with increasing ϕ and becomes negligible at around $\phi \approx 40°$. The simulated cross-sectional scans of a sample SWNT using two different values of ϕ show that the image can be distorted and shifted laterally when ϕ is large, in some cases giving measured heights appreciably *greater* than the sample dimensions. We show analytically that the tip−sample forces that occur during imaging can be significantly lower when CNT probes are used instead of conventional probes, even in the absence of buckling, and that they can be further reduced by increasing ϕ. On the basis of this result, we propose the design of free-standing kinked probes for the characterization of sensitive samples, whereby the probe approaches the sample at a vertical orientation and possesses a tilted section that regulates the tip−sample interaction forces.

1. Introduction

Carbon nanotube (CNT) AFM probes have shown a significant potential for high-resolution imaging due to their nanoscale dimensions, high aspect ratio, stiffness, and chemical stability.[1−11] Various fabrication processes are available to manufacture CNTs and attach them to conventional AFM tips.[1,2,4−6,12−15] Although these methods are reliable and repeatable, challenges still exist in manufacturing probes that are capable of high-quality imaging. It has been reported that the probe tilt angle with respect to the axis normal to the substrate, ϕ, is one of the most critical parameters affecting probe quality and that it must be below approximately 30° for high-quality imaging to be possible.[1,10,11,15,17,18] In general, probe quality decreases as ϕ increases, and the ideal probe has $\phi = 0°$. However, there has been little *quantitative* investigation of the effect of ϕ *on image quality* for CNT probe diameters greater than 1 nm and on whether modulation of this parameter can be advantageous.

We have previously described a methodology that combines molecular dynamics (MD) and classical dynamics (CD) to simulate tapping-mode AFM imaging.[19] With this method, one first calculates the forces and geometry changes experienced by the probe and the sample during imaging using MD. The tip−sample interaction forces are then integrated into the equation of motion of the oscillating cantilever to simulate the AFM operation and the construction of the image. This analysis treats the cantilever−tip ensemble as a point mass using the equation of motion of a damped harmonic oscillator, which has been used extensively to study these systems:[20]

$$m\frac{d^2z(Z_c,t)}{dt^2} = -kz(Z_c,t) - m\frac{\omega_o}{Q}\frac{dz(Z_c,t)}{dt} + F_{ts}(z_{ts}) + F_o\cos(\omega t) \quad (1)$$

where $z(Z_c,t)$ is the instantaneous tip position with respect to the AFM cantilever rest position (Z_c), k the harmonic force constant for the displacement of the tip with respect to Z_c, m the cantilever's effective mass, $\omega_0 = (k/m)^{1/2}$ the free resonant frequency, Q the quality factor, z_{ts} the instantaneous tip *vertical* position *with respect to the sample*, $F_{ts}(z_{ts})$ the *vertical component* of the tip−sample interaction force (calculated using MD), and $F_o\cos(\omega t)$ the oscillating driving force applied to the cantilever. We used $Q = 150$, $k = 4.8$ N/m, and $\omega_o = 47.48$ kHz for all calculations described here, corresponding to previously reported experimental and theoretical results.[19]

Using a 40,40 single-wall carbon nanotube (SWNT) probe model constructed from the TEM image of an actual probe[19] (diameter 5.5 and aspect ratio 7.5, Figure 1), we first study the effect of ϕ on $F_{ts}(z_{ts})$ and its gradient upon contact with a Si(100)−OH surface. We show that the vertical probe stiffness, which we quantify as the maximum absolute value of the gradient of $F_{ts}(z_{ts})$ with respect to z_{ts} at the onset of lateral probe slippage, decreases linearly with increasing ϕ up to approximately $\phi = 40°$, beyond which it becomes negligible. We

* To whom correspondence should be addressed. E-mail: wag@wag.caltech.edu.

10.1021/jp052758g CCC: $30.25
Published on Web 08/09/2005

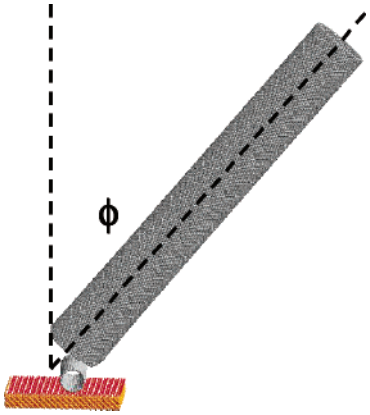

Figure 1. Model (32000 atoms) of a 40,40 SWNT probe, constructed from the TEM image of an actual probe,[19] interacting with a 16,16 SWNT sample on a Si(100)−OH surface. The probe diameter and length are 5.5 and 40 nm, respectively, and $\phi = 40°$. The sample is a 16,16 SWNT with diameter and length of 2.1 and 10 nm, respectively, whose ends were held fixed during imaging.

repeat the analysis for single-, double-, and triple-wall CNT probe models (multiwall nanotubes, MWNTs), all with an outer diameter of 3.4 nm and aspect ratio of 7.5, and find that the MWNT probe stiffness is proportional to the number of walls but that the difference in stiffness between SWNT and MWNT probes decreases linearly as ϕ increases and becomes negligible beyond approximately $\phi = 40°$. Using the 40,40 SWNT probe model with $\phi = 40°$, we simulate the tapping-mode AFM cross-sectional scan of a 16,16 SWNT (diameter 2.1 nm) lying prone on the surface and compare it to a previously reported high-quality image obtained for $\phi = 15°$, which was shown to be in agreement with the experimental result.[19] This comparison illustrates the lateral image shifting and measured height distortion that take place as ϕ increases and shows that it is primarily the result of *simultaneous* contact between the probe and the sample *and* between the probe and the substrate, which reduces the probe's ability to bend. Finally, we describe tapping-mode AFM simulations based on eq 1 for SWNT probes with different values of ϕ, which quantify its effect on the cantilever oscillation dynamics in terms of forces, oscillation amplitudes, and probe deformation, and compare the results to those obtained with a conventional 15 nm radius Si tip. We find that the tip−sample repulsive forces during imaging can be several times greater for Si tips than for CNT tips, even in the absence of buckling, and explain this difference in terms of the area under the tip−sample force curve, which corresponds to work used to stop the downward motion of the AFM cantilever as it approaches the surface every oscillation [This comparison focuses primarily on Si tips of conventional dimensions (i.e., with radii >5 nm), which are the most common. However, in the Supporting Information we provide calculations which suggest that if Si tips of dimensions comparable to those of SWNTs can be manufactured and maintained sharp during imaging, they can also lead to lower tip−sample interaction forces that are similar to those obtained with vertically aligned SWNTs.]

Our results confirm the general conclusions of previous experimental and theoretical studies indicating that the optimum probe orientation is along the axis normal to the substrate surface, but they also suggest that probe stiffness can be modulated by controlling the tilt angle, thus enabling the tapping-mode AFM characterization of highly sensitive samples, which are damaged by large tip−sample forces. We propose that the ideal probe to image such sensitive samples is a *free-standing* kinked probe (Figure 2) that approaches the sample at a nearly vertical orientation, thus ensuring high imaging resolution, and contains a tilted section that modulates the tip−sample interaction forces. We discuss current alternatives in manufacturing these probes and offer our design as a challenge to experimental research groups.

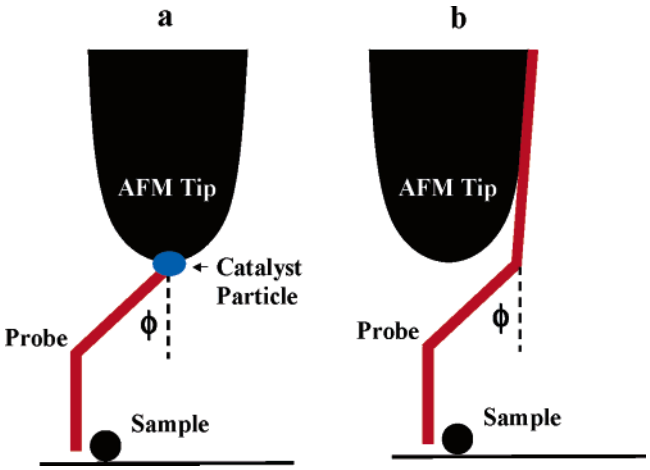

Figure 2. Illustration of *free-standing* kinked nanotube AFM probes containing a tilted section that acts as a spring, which modulates the tip−sample interaction force and a vertical section that ensures high imaging resolution. (a) Probe grown from a catalyst particle on the supporting tip. (b) Probe adsorbed onto the supporting tip.

2. Methods

A detailed description of the MD/CD AFM methods, force field functional forms and parameters, and simulation software is provided in ref 19. All tip−sample interaction force curves described here were constructed using *fully atomistic* models containing up to 32000 atoms.

Note that throughout this paper "probe stiffness" refers to the *effective* stiffness of the probe in the vertical direction (eq 1 is a *one-dimensional* equation describing the AFM cantilever motion only in the *vertical* direction).

2.1. SWNT and MWNT Probe Stiffness. To study the effect of ϕ on SWNT probe stiffness, we calculated the tip−sample interaction force as a function of the vertical tip position [$F_{ts}(z_{ts})$ in eq 1] for the 40,40 SWNT probe in Figure 1 (diameter 5.5 nm and length 40 nm) approaching a Si(100)−OH surface, using values of ϕ ranging from 0° to 60° at increments of 10°. We then calculated the gradient of these functions and determined the "terminal force gradient", which we define as the steepest value of the tip−sample force gradient observed when the probe is compressed against the surface (Figure 3 shows that the force curves for SWNT probes approach straight lines at the points of probe slippage, suggesting that the terminal force gradient can be used as a quantitative parameter in the description of CNT probe stiffness).

To quantify the dependence of probe stiffness on ϕ and the number of walls in MWNT probes, we constructed the tip−sample force curves for single-, double-, and triple-wall CNT probes of the same outer diameter and length (3.4 and 25 nm, respectively) imaging a Si(100)−OH surface for $\phi = 10°$, 25°, and 40° and calculated their terminal force gradient. In all three cases, the outermost wall was modeled as a 25,25 SWNT (diameter 3.4 nm) and the inner walls were modeled as 20,20 (diameter 2.7 nm) and 15,15 (diameter 2.0 nm) SWNTs, as appropriate. The difference in diameters between adjacent probe walls was selected to fit the known interlayer distance in MWNTs (~0.35 nm).

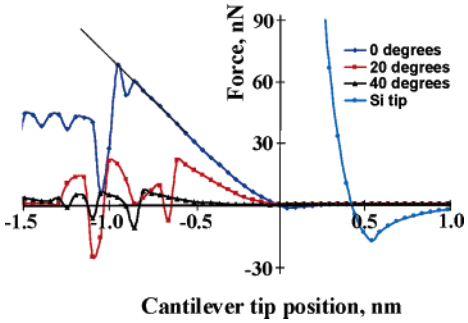

Figure 3. Tip−sample interaction force vs cantilever tip position for the 40,40 SWNT probe shown in Figure 1 (for $\phi = 0°$, 20°, and 40°) and for a 15 nm radius Si tip imaging a Si(100)−OH surface. The results indicate that, for the SWNT probe, the tip−sample force and its steepness decrease with increasing ϕ in the region of tip−sample contact. The dotted line on the 0° curve illustrates the extrapolation of the force curve beyond the point of probe slippage, whose slope we define as the terminal force gradient and use as a quantitative measure of probe stiffness. The discontinuities in the SWNT force curves are due to lateral probe slippage, as illustrated in Figure 4. Negative values of the tip position indicate tip and sample deformation.

To provide a comparison between CNT and conventional AFM tips, we also calculated $F_{ts}(z_{ts})$ for a 15 nm radius Si tip imaging the same Si(100)−OH surface [We are primarily interested in providing a general comparison between SWNT tips and Si tips of radii greater than 5 nm, which are the most common. However, we did perform a comparison between a 30,30 SWNT tip and a Si tip of the same radius (∼1.7 nm) and provide the results and general conclusions in the Supporting Information.]

2.2. Image Distortion for Highly Tilted Probes. To study the distortion of a real image as ϕ increases, we calculated the AFM cross-sectional scan of a 16,16 SWNT lying prone on a Si(100)−OH surface using the probe model shown in Figure 1 with $\phi = 40°$ and plotted it on the same graph with a previously reported calculation performed on the same model but with $\phi = 15°$, which gave a high-quality image in agreement with the experimental result.[19] These cross-sectional scans were constructed using a free oscillation amplitude $A_o = 39$ nm, and an amplitude set point of 15.4 nm. Reference 19 provides the details of the theoretical procedure used to construct the images.

2.3. Cantilever Oscillation Dynamics. Here we constructed the oscillation amplitude curves (vs cantilever rest position with respect to the surface, Z_c) for the 40,40 SWNT probe for $\phi = 0°$, 20°, 30°, and 40° and for free oscillation amplitudes $A_o = 20$, 30, and 40 nm. This was done by inserting the force curves described in section 2.1 into eq 1 and solving numerically for the tip position as a function of time, from which the oscillation amplitude is directly obtained. Since probe slippage occurred at low tip−sample forces for $\phi = 40°$, we extrapolated the smooth portion of the corresponding force curve beyond the point of slippage using the terminal force gradient (as illustrated in Figure 3) to be able to compare the results to those obtained for lower values of ϕ, for which slippage did not occur during imaging. From the tip trajectory and the tip−sample force curves we also calculated the lowest vertical position of the AFM cantilever tip, Z_{min}, and the maximum tip−sample force, F_{max}, observed *during one full cantilever oscillation* for different values of Z_c (for these systems F_{max} occurs at Z_{min}, where the tip and sample experience the greatest deformation). We also calculated $z(Z_c,t)$, $Z_{min}(Z_c)$, $F_{max}(Z_c)$, and the oscillation amplitude (vs Z_c) for the Si tip, using the same three values of A_o.

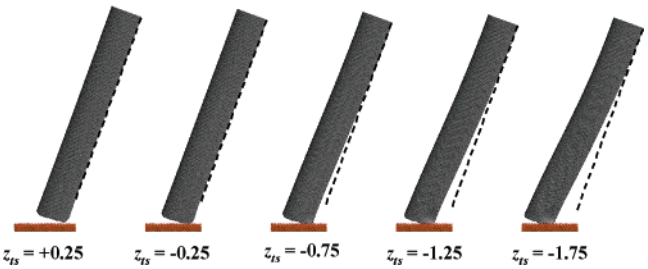

Figure 4. Snapshots of the 40,40 SWNT probe shown in Figure 1 approaching a clean Si(100)−OH surface for different values of z_{ts}. The probe tilt angle is 20°. The pictures show that significant bending and lateral slipping take place when the probe descends below $z_{ts} = -0.75$ nm. This causes discontinuities in the tip−sample interaction force curves, as shown in Figure 3.

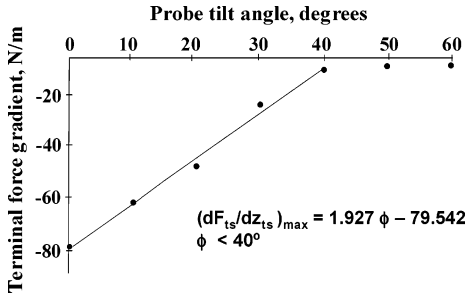

Figure 5. Terminal force gradient vs ϕ for the 40,40 SWNT probe shown in Figure 1 imaging a Si(100)−OH surface. *Increasingly negative* gradients correspond to *greater* vertical probe stiffness. The graph has two well-defined regions, in which the terminal force gradient varies approximately linearly with ϕ. For $\phi < 40°$, it varies with a slope of ∼1.93 (N/m)/deg, and for $\phi > 40°$, it approaches the horizontal axis.

3. Results

3.1. SWNT and MWNT Probe Stiffness. Figure 3 shows the calculated tip−sample interaction force curves for the 40,40 SWNT probe (for $\phi = 0°$, 20°, and 40°) and for the 15 nm radius Si tip imaging a Si(100)−OH surface. The graph shows that when using the SWNT probe, the tip−sample force decreases with increasing ϕ for tip positions below the point of initial tip−sample contact (zero on the horizontal axis). It also shows that the smooth section of the force curve approaches a straight line as the cantilever descends significantly beyond the contact point, up to the point of lateral probe slippage (illustrated in Figure 4), beyond which it oscillates in an unpredictable fashion. As ϕ increases, the terminal force gradient becomes less steep, indicating a reduction in probe stiffness. The force curve for the Si tip is the steepest of all due to the significantly more repulsive tip−sample interaction forces experienced by this solid and less deformable probe [In the Supporting Information we provide a comparison between the force curves of a 30,30 SWNT tip and a Si tip of the same radius (∼1.7 nm), which shows that the tip−sample repulsive forces are comparable in both cases. Since such fine tips are not the most commonly used in AFM, and since the focus of our study is CNT probes, we restrict our discussion to Si tips with radii greater than 5 nm.] Figure 5 shows the smooth linear behavior of the terminal force gradient as a function of ϕ for the SWNT probe, suggesting that it is an ideal measure of CNT probe stiffness. There are two well-defined regions on the graph; in both the terminal force gradient varies approximately linearly with ϕ. In the first region, where $\phi < 40°$, it varies with a slope of ∼1.93 (N/m)/deg, and in the region where $\phi > 40°$, it is negligible. Thus, if ϕ can be controlled, stiffness modulation is possible for $\phi < 40°$ (but not for $\phi > 40°$).

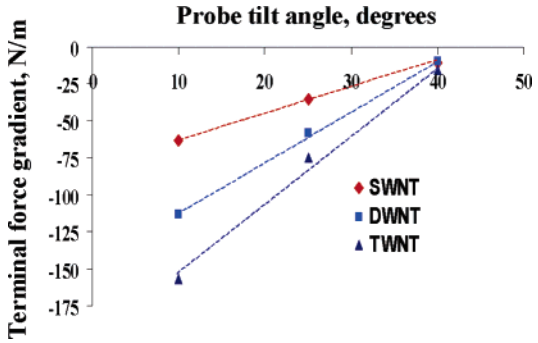

Figure 6. Terminal force gradient vs ϕ for single-, double-, and triple-wall CNT probes (SWNT, DWNT, and TWNT, respectively) with an outer diameter and length of 3.4 and 25 nm, respectively, and interwall spacing of 0.35 nm. MWNT probe stiffness is proportional to the number of walls, but the difference in stiffness between probes containing a different number of walls decreases as ϕ increases and becomes negligible at approximately $\phi = 40°$.

Our calculations also indicate that the maximum force a CNT probe can withstand without slipping on a clean and dry Si(100)−OH surface rapidly decreases with increasing tilt angle. For example, Figure 3 shows that this force drops from ~68 to only ~22 nN when ϕ is increased from 0° to 20° for our 40,40 SWNT probe. These values could change for other surfaces or when moisture and impurities are present on the surface, but even in those cases, we expect the *general* trend to be similar.

Figure 6 shows the terminal force gradient vs ϕ for single-, double-, and triple-wall CNT probes with an outer diameter and length of 3.4 and 25 nm, respectively (the corresponding force curves for MWNTs are provided in the Supporting Information). The results clearly show that MWNT probes with increasing number of walls are stiffer in the vertical direction when compared to SWNT probes, with the probe stiffness being proportional to the number of walls. However, the difference in stiffness between SWNT and MWNT probes decreases linearly as ϕ increases and becomes negligible at approximately $\phi = 40°$.

Our simulations show that the primary modes of tip deformation in our systems (see the Supporting Information) are macroscopic bending/shearing and local deformation at the end of the tip (shearing occurs because only one corner of the CNT tip contacts the surface when the probe is tilted). We found that the proportion of strain energy stored in the *local* deformation mode with respect to the macroscopic bending/shearing mode is greater for tilted probes than for vertical probes. For example, we calculated that, for a tip position of −0.5 nm (measured on the horizontal axis of Figure 3) and when $\phi = 0°$, approximately 20% of the *total* strain energy of the 40,40 SWNT tip is stored in the 4 nm at the end of the probe (i.e., in 10% of the total probe length). This proportion increases to ~26% when $\phi = 10°$ and to ~64% when $\phi = 20°$ and then decreases slightly for $\phi > 20°$. This may be counterintuitive, since one would expect that, as the probe tilt increases, it becomes much easier to bend and that this would cause more strain energy to be stored in the bending mode. However, in the range of tip positions useful for imaging (cantilever tip positions >−0.75 in Figure 3), the *lateral* deformation of the wall at the end of the tip can be significant due to the hollow nature of CNTs. This is more significant for SWNTs than MWNTs.

3.2. Image Distortion for Highly Tilted Probes. Figure 7 shows the simulated AFM cross-sectional scans of a 16,16 SWNT lying prone on the surface obtained with the 40,40 SWNT probe at $\phi = 15°$ (previously shown to be in agreement

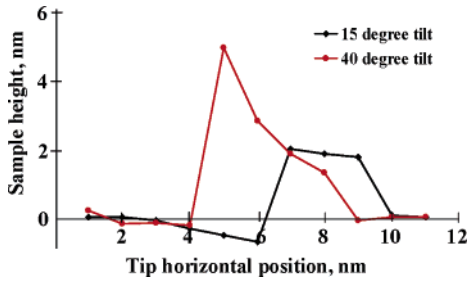

Figure 7. Simulated AFM cross-sectional scan (sample height vs horizontal position) of a 16,16 SWNT (2.1 nm diameter) lying prone on a Si(100)−OH surface, obtained using the 40,40 SWNT probe model shown in Figure 1 for $\phi = 15°$ and 40°. A high-quality image was obtained for $\phi = 15°$, in agreement with the experimental result,[19] but not for $\phi = 40°$.

Figure 8. A 40,40 SWNT probe imaging a prone 16,16 SWNT at $\phi = 40°$ showing that this tilt angle is inappropriate because it allows the probe to contact the surface *and* the sample at different horizontal positions *simultaneously*. This type of inappropriate contact causes severe lateral shifting and size distortion of the AFM image, as depicted in Figure 7.

with experiment[19]) and at $\phi = 40°$. The result obtained for $\phi = 40°$ shows a distortion in the geometry of the sample with a significant discrepancy between the calculated and the actual dimensions. MD simulations indicate that the peak in the scan at a horizontal position of 5 nm (showing a measured height of over twice the actual sample height) occurs because the probe is able to contact the sample and the substrate surface simultaneously (Figure 8), which reduces its effective flexibility. The observed distortion in the sample height is counterintuitive. Normally one would expect a softer probe to be less sensitive to the sample details, which would result in *reduced* measured height. However, as the probe contacts the surface and the sample simultaneously, the repulsive interactions with the sample exert vertical (upward) forces on the side of the probe that reduce its ability to bend downward upon contacting the surface. This results in a greater *effective* probe stiffness (analogous to that of a shorter probe), which opposes the descent of the oscillating cantilever more strongly than if the sample were not present and the probe were only contacting the surface. The net result is a higher reading in a region where the *end* of the SWNT probe is *not* contacting the sample and should not be able to detect it. This type of inappropriate tip−sample contact can also shift the image to the left with respect to the case when a nearly vertical probe is used because the probe can sense the presence of the sample before its imaging end reaches the same horizontal position as the edge of the sample (when traveling from left to right). The right side of the image is similar for both tilt angles, indicating that, for this type of sample, the deterioration of the image for high tilt angles is *primarily* due to geometric incompatibility between the probe and sample. The results of sections 3.1 and 3.3 show that the decrease in probe stiffness and the occurrence of lateral slippage are also significant for $\phi = 40°$. From these results it is evident

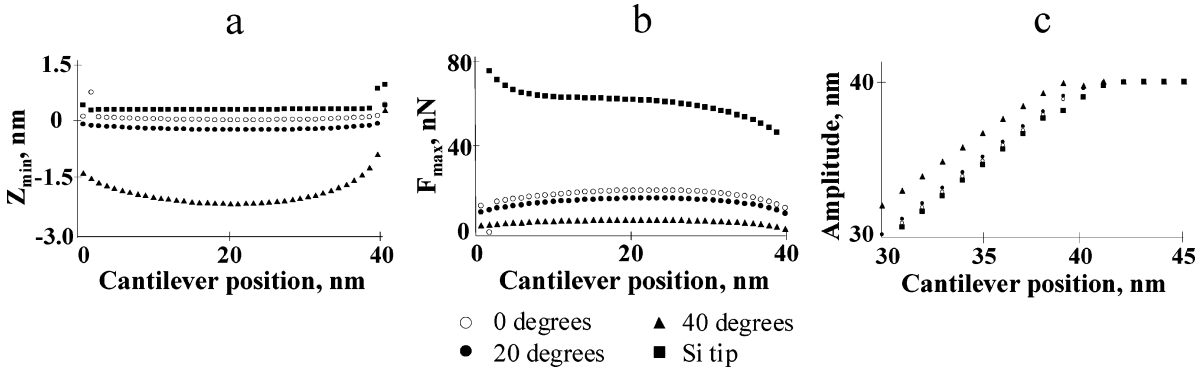

Figure 9. Lowest cantilever position (a) and maximum tip−sample force (b) observed *during one full oscillation of the AFM cantilever* and oscillation amplitude (c) vs cantilever rest position, for the 40,40 SWNT probe shown in Figure 1 (for $\phi = 0°$, 20°, and 40°) and for a 15 nm radius Si tip imaging a clean Si(100)−OH surface. $A_o = 40$ nm in all cases. The discontinuities on the curves (such as the jump in the Z_{min} curve for the Si tip (black squares) between cantilever positions of 38 and 39 nm) correspond to the well-known transitions between the attractive and repulsive imaging regimes of tapping-mode AFM.[21] [Note that $Z_{min} = 0$ corresponds to the AFM cantilever rest position for which the tip (SWNT or Si) is *first* able to contact the surface.]

that modulation of probe stiffness cannot be successfully accomplished unless the probe approaches the sample at a nearly vertical orientation.

3.3. Cantilever Oscillation Dynamics. Figure 9 illustrates the dependence of Z_{min}, F_{max}, and the cantilever oscillation amplitude on the cantilever rest position for the 40,40 SWNT probe and for the 15 nm radius Si tip imaging a Si(100)−OH surface with $A_o = 40$ nm. As ϕ increases for the SWNT probe, its lower vertical stiffness allows the cantilever to approach the surface more closely (reaching lower values of Z_{min}) and oscillate with greater amplitude. This also causes greater probe bending, as verified through MD simulations. Note that the separation between curves for $\phi = 0°$ and $\phi = 20°$ is much smaller than the separation between the curves for $\phi = 20°$ and $\phi = 40°$, indicating that the sensitivity of Z_{min}, F_{max}, and the cantilever oscillation amplitude to changes in ϕ increases as ϕ increases.

Various authors have pointed out that the degree of sample damage is lower when using CNT tips vs conventional Si tips because the maximum tip−sample force is limited by CNT buckling,[3−5] but our results show that the tip−sample forces for CNT probes are also lower *in the absence of buckling* and that this is due to the difference in steepness between the tip−sample force curves of CNT and Si tips (Figure 3). (The results provided in section 1 of the Supporting Information show that lower tip−sample forces can also be obtained through the use of ultrafine Si tips. The discussion presented here is limited to Si tips of radii greater than 5 nm.) As the repulsive portion of the force curve becomes *less* steep, the area under the curve from the point of initial tip−sample contact up to a *fixed* value of F_{max} increases. Since this area represents work used to stop the downward motion of the oscillating cantilever and since the work requirement does not vary significantly with the shape of the force curve, the necessary work (area) can be obtained for a lower value of F_{max} with a *less* steep force curve. Figure 3 shows that the force curve for the Si tip is significantly steeper than any of the force curves for the SWNT tip, and Figure 9b confirms that during imaging this leads to tip−sample forces several times greater for the Si tip. As ϕ increases, the force curves for the SWNT probe become less steep, which results in lower values of F_{max} for greater values of ϕ. Thus, we expect a reduction in the degree of sample damage as ϕ increases, *even when there is no change in the imaging parameters*.

Note that we did *not* observe buckling in any of our simulations with 40,40 SWNT vertical probes experiencing repulsive forces up to ∼68 nN, which are over 3 times greater than those observed during imaging with $A_o = 40$ nm (Figure 9b). For this value of A_o buckling was *not* observed for any probe tilted less than 30°, although moderate bending did take place for $\phi > 20°$. Consider, for example, the 40,40 SWNT probe tilted 20°. Figure 9b shows that when $A_o = 40$ nm, the maximum tip−sample forces are ∼16.5 nN. Figure 3 shows that for this tilt angle slippage did not occur below ∼23 nN (the force curve is smooth up to this value), which according to Figure 4 corresponds to only *minor* bending.

The behavior of Z_{min}, F_{max}, and the cantilever oscillation amplitude for $A_o = 20$ and 30 nm (Supporting Information) shows a dependence on ϕ similar to that for $A_o = 40$ nm (Figure 9), but the observed variations for different values of ϕ are smaller due to the smaller excitation force required to obtain smaller values of A_o. As expected the oscillation amplitude and F_{max} increased with increasing A_o (due to a greater cantilever excitation force), while Z_{min} decreased (due to increased tip and sample deformation).

4. Discussion

4.1. Shortcomings of Highly Tilted Probes. One of the standard criteria used to select AFM CNT probes is that their tilt angle must be as close as possible to zero with respect to the axis normal to the sample substrate.[1,15,17,18] Experiments conducted using a wide range of probe sizes and theoretical simulations of 1 nm diameter probes indicate that the image can be significantly distorted when this angle is greater than 30°.[1,17,18] Our simulations confirm this conclusion for a wider range of probe dimensions and provide a quantitative measure of the decrease in vertical probe stiffness as the tilt angle increases. (Note that the dimensions of the probes used in our analysis were selected to be in the range of high-quality AFM probes,[1] thus excluding the most obvious causes of imaging artifacts and isolating the effect of the probe tilt angle on image quality. However, we do believe that there are other parameters, such as the probe aspect ratio, which can be tuned/optimized to modulate the tip−sample forces, although with a smaller effect than that of adjusting the tilt angle.) The results show that the distortion of the image for highly tilted probes is due to the combination of four main factors.

First, as ϕ increases the probe stiffness (as defined in section 1) decreases linearly (Figures 3 and 5), making the probe less sensitive to the fine details of the sample. This is similar to using a sponge probe, whose softness would mask the features of the sample, causing it to appear flat.

Second, as a result of its lower stiffness, the probe is less capable of limiting the range of oscillation of the AFM

cantilever, which can lead to probe bending, lateral slipping, and even buckling. Consider, for example, the results of Figure 9a for the 40,40 SWNT probe. The chart shows that when $\phi = 40°$ and $A_o = 40$ nm, the cantilever descends below a position of -0.75 nm during every oscillation for most of the range of cantilever rest positions shown, but according to Figure 3 this results in slippage.

Third, as ϕ increases the likelihood that the geometry of the tip and the sample are incompatible increases. This is the case for SWNT samples, for which a highly tilted probe is able to contact the sample and the substrate surface simultaneously (Figure 8), causing significant distortions and lateral shifting of the image (Figure 7).

Finally, at high tilt angles the supporting Si tip approaches the sample more closely for a given CNT probe length, experiencing greater interactions with the surface and in some cases causing imaging artifacts such as shadowing.[1] This is magnified when severe probe bending and buckling occur. Consider, for example, a 40,40 SWNT probe protruding 10 nm from a 15 nm radius Si tip tapping at the bottom of a narrow, 4 nm deep trench. Our calculations show that when $A_o = 10$ nm and $\phi = 40°$, the *maximum* repulsive force experienced by the SWNT tip will be ~6.5 nN. Under these conditions, the supporting Si tip can experience attractive forces as large as 2% of this value, which compares to only 0.3% when $\phi = 0°$. These interactions can be quite significant if one considers that the *repulsive* forces between the CNT probe and the surface act over a very small range (<0.25 nm) and that the attractive forces between the Si tip and the surface act over very long ranges (>1 nm) and are significantly greater than the *attractive* forces between the CNT probe and the surface (Figure 3).

Our results show that MWNT probes exhibit greater vertical stiffness than SWNT probes, making them significantly more robust at nearly vertical orientations. However, since this advantage vanishes as ϕ increases and since the outer geometry of MWNTs does not differ from that of SWNTs, MWNTs cannot overcome the deterioration in imaging quality associated with highly tilted probes ($\phi > 40°$).

4.2. Imaging of Sensitive Samples. We have shown analytically that the tip−sample repulsive forces that take place during tapping-mode AFM imaging can be significantly lowered when CNT tips are used instead of conventional AFM tips. However, it is well-known that there is a wide range of organic and biological samples that could be damaged in contact-mode AFM regimes even when using CNT tips, for which further modulation of the tip−sample forces would be advantageous. Various authors have successfully imaged sensitive samples in noncontact mode,[5,7,8] but this type of imaging has two very important limitations: first, it may be subject to tip-induced broadening[3,16] caused by the long-range van der Waals forces between the tip and the sample, and second, since there is no tip−sample contact, one can only obtain information about the bulk geometry of the sample but not about its elastic properties.

Some biological samples have been successfully imaged in contact mode,[3,4,6,10,11,14,16] but this is generally difficult to accomplish with conventional CNT probes because the range of probe sizes (and stiffness) is limited by the type and size of CNTs that can be controllably manufactured and attached to AFM tips. Additionally, the softer (smaller) CNT probes that would be required to image the softest samples may not be suitable for imaging due to aspect ratio limitations (they would have to be extremely short to reduce bending and prevent buckling, and this could cause interference by the supporting Si tip).

It has also been reported that imaging in a liquid environment facilitates tapping-mode AFM imaging,[16] but this may change the conformation of the sample and affect the tip−sample interactions in a way that precludes imaging in the desired state, especially for nonbiological samples. Furthermore, since nonfunctionalized CNTs are hydrophobic, imaging in an aqueous environment (the most common environment in biological applications) is not always feasible.[22] (The simulated force curve of a 1.7 nm radius Si tip, provided in the Supporting Information, shows that such fine tips could provide an alternative for imaging sensitive samples in aqueous environments.)

Thus, to further develop the tapping-mode AFM imaging techniques for soft samples, it is necessary to explore new designs and manufacturing methods that can produce softer CNT probes of controlled stiffness.

4.3. Challenges and Alternatives. We have shown that CNT probe stiffness can be modulated through adjustments in ϕ, which presents an opportunity for designing probes of the appropriate stiffness for each type of sample. However, to not compromise image quality, any new probe design must meet several important criteria. First, it is necessary that the probe approach the sample at a nearly vertical orientation so that the artifacts described by Figures 7 and 8 do not take place. Second, it is necessary that imaging take place under conditions that do not lead to severe bending or buckling (this may require using lower values of A_o for higher values of ϕ). Third, the AFM probe must be long enough that the supporting silicon tip does not approach the surface too closely during imaging. Fourth, it is necessary that the probe stiffness be sufficiently high (as stiff as the sample allows) that the topography of the sample does not get absorbed in the compliance of the probe (a softer probe will cause less damage to the sample, but it will also provide a flatter image and vice versa). And finally, it is necessary that the CNT probe be well immobilized on the supporting Si tip so that its length and orientation do not change during imaging.

The obvious challenge here is the feasibility of manufacturing softer probes that meet such stringent criteria. Conventional methods to attach straight CNTs to conventional tips offer some versatility, but do not offer a complete solution. Although controlling the probe tilt angle during fabrication is possible with the pore-growth[2] and some of the manual-assembly[6,13] methods, straight, tilted probes do not offer the best imaging resolution because they do not approach the sample at the ideal vertical orientation. To overcome this challenge, we propose the design and manufacturing of *free-standing* kinked nanotube[23] or nanowire probes (Figure 2), containing a tilted section that modulates stiffness and a vertical section that ensures high imaging resolution. Our results suggest that probes of this type would enable high-quality imaging of delicate samples without the limitations of either highly tilted or too stiff probes.

Manufacturing kinked AFM probes reliably also presents significant challenges, and to our knowledge this has not yet been accomplished. However, we have found in the literature two methodologies that can produce probes of controlled orientation and which could, at least in principle, be modified to grow probes with the desired geometry. Ye et al.[13] have recently reported on an innovative bottom-up approach to manufacturing AFM probes using plasma-assisted chemical vapor deposition, whereby probe growth is directed by an electric field at locations that have been predetermined through nanopatterning of a Si wafer with the catalyst material. After probe growth, the AFM cantilevers are cut to the desired dimensions using micromachining procedures. The smallest probe diameter that has been reported for this procedure is

between 40 and 80 nm, but the authors believe that smaller probes could be obtained by utilizing smaller catalyst particles.[13] Tay and co-workers[24] have also reported on a procedure that allows the manufacturing of probes of controlled orientation, using a field emission method to grow tungsten and cobalt (and potentially composite material) nanowires of the desired length and thickness on conventional AFM tips, thus providing an alternative to CNTs. We also believe that the probe design shown in Figure 2b could be manufactured by controllably growing kinked nanotubes on a substrate (using a process similar to that of Ye et al.,[13] perhaps with adjustments in the direction of the electrical field or with the introduction of trace amounts of atoms other than carbon during CNT growth to produce the kinks) and then attaching them to the supporting Si tip via the pickup method,[14] followed by electrical pulse etching[5] to shorten them to the desired dimensions. This method would have the advantage of decoupling nanotube growth from AFM probe manufacturing.

We present our design as a challenge to experimental groups and highly encourage developments in this area, even for samples that are not susceptible to damage by stiff vertical probes. Tapping-mode AFM imaging with probes of varying stiffness could provide, for example, information on the maximum force that the sample is able to withstand without damage and on the difference in stiffness between the sample as a whole and its features. This type of characterization could also be used to selectively image internal (subsurface) features of multilayered samples. Finally, there may be other types of probe microscopy, such as chemical force microscopy and scanning tunneling microscopy, where ultrasoft probes could also be useful in minimizing sample damage during imaging.

5. Conclusions

We have investigated the quantitative dependence of the tip−sample interaction forces for single-wall and multiwall nanotube AFM probes on their tilt angle with respect to the axis normal to the sample substrate, describing the cantilever dynamics and image distortion mechanisms that can occur when this angle is large. We have also shown that the tip−sample forces that occur during imaging can be significantly lower when using carbon nanotube probes than when using conventional AFM probes (even in the absence of nanotube probe buckling) and explained the difference in terms of the area under the tip−sample interaction force curve. Our results confirm that the ideal probe orientation for nonsensitive samples is along the axis normal to the sample substrate and provide relationships between probe stiffness and tilt angle for single-wall and multiwall nanotube AFM probes of diameters between 3.5 and 5.5 nm. For sensitive samples, we have proposed and discussed the design of specialized kinked AFM probes, whereby probe stiffness is modulated through control of the tilt angle of a section of the probe.

Acknowledgment. We gratefully acknowledge the contribution of Professor Konstantinos P. Giapis to the probe designs shown in Figure 2 and of Lawrence A. Wade and Professor C. Patrick Collier in revising and discussing the manuscript.

Supporting Information Available: Comparison of force curves between single-wall carbon nanotube and Si tips of comparable radius, force curves for single-, double- and triple-wall carbon nanotube probes, cantilever oscillation dynamics for $A_o = 20$ nm, and analysis of tip deformation modes. This material is available free of charge via the Internet at http://pubs.acs.org.

References and Notes

(1) Wade, L. A.; Shapiro, I. R.; Ma, Z.; Quake, S. R.; Collier, C. P. *Nano Lett.* **2004**, *4*, 725.

(2) Hafner, J. H.; Cheung, C. L.; Woolley, A. T.; Lieber, C. M. *Prog. Biophys. Mol. Biol.* **2001**, *77*, 73.

(3) Umemura, K.; Komatsu, J.; Uchihashi, T.; Choi, N.; Ikwawa, S.; Nishinaka, T.; Shibata, T.; Nakayama, Y.; Katsura, S.; Mizuno, A.; Tokumoto, H.; Ishikawa, M.; Kuroda, R. *Biochem. Biophys. Res. Commun.* **2001**, *281*, 390.

(4) Nishijima, H.; Kamo, S.; Akita, S.; Nakayama, Y. *Appl. Phys. Lett.* **1999**, *74*, 4061.

(5) Wong, S. S.; Harper, J. D.; Lansbury, P. T.; Lieber, C. M. *J. Am. Chem. Soc.* **1998**, *120*, 603.

(6) Uchihashi, T.; Choi, N.; Tanigawa, M.; Ashino, M.; Sugawara, Y.; Nishijama, H.; Akita, S.; Nakayama, Y.; Tokumoto, H.; Yokoyama, K.; Morita, S.; Ishikawa, M. *Jpn. J. Appl. Phys.* **2000**, *8B*, L887.

(7) Maeda, Y.; Nishijima, H.; Akita, S.; Matsumoto, T.; Nakayama, Y.; Kawai, T. *Jpn. J. Appl. Phys.* **2001**, *40*, 1425.

(8) Bunch, J. S.; Rhodin, T. N.; McEuen, P. L. *Nanotechnology* **2004**, *15*, S76.

(9) Chang, Y. C.; Chang, C. S.; Wang, D. C.; Lee, M.-H.; Wang, T.-F.; Wu, M.-Y.; Fu, T.-Y.; Tsong, T. T. *Jpn. J. Appl. Phys.* **2004**, *43*, 4517.

(10) Woolley, A. T.; Cheung, C. L.; Hafner, J. H.; Lieber, C. M. *Chem. Biol.* **2000**, *7*, R193.

(11) Hohmura, K. I.; Itokazu, Y.; Yoshimura, S. H.; Mizuguchi, G.; Masamura, Y.; Takeyasu, K.; Shiomi, Y.; Tsurimoto, T.; Nishijima, H.; Akita, S.; Nakayama, Y. *J. Electron Microsc.* **2000**, *49*, 415.

(12) Hafner, J. H.; Cheung, C. L.; Lieber, C. M. *J. Am. Chem. Soc.* **1999**, *121*, 9750.

(13) Ye, Q.; Cassell, A. M.; Liu, H.; Chao, K.-J.; Han, J.; Meyyappan, M. *Nano Lett.* **2004**, *4*, 1301.

(14) Hafner, J. H.; Cheung, C. L.; Oosterkamp, T. H.; Lieber, C. M. *J. Phys. Chem. B* **2001**, *105*, 743.

(15) Song, W. Y.; Jung, K. Y.; O, B.-H. *Rev. Sci. Instrum.* **2005**, *76*, 025107.

(16) Chen, L.; Cheung, C. L.; Ashby, P. D.; Lieber, C. M. *Nano Lett.* **2004**, *4*, 1725.

(17) Snow E. S.; Campbell, P. M.; Novak, J. P. *J. Vac. Sci. Technol., B* **2002**, *20*, 822.

(18) Snow E. S.; Cambell, P. M.; Novak, J. P. *Appl. Phys. Lett.* **2002**, *80*, 2002.

(19) Shapiro, I. R.; Solares, S. D.; Esplandiu, M. J.; Wade, L. A.; Goddard, W. A.; Collier, C. P. *J. Phys. Chem. B* **2004**, *108*, 13613.

(20) Garcia, R.; San Paulo, A. *Phys. Rev. B* **1999**, *60*, 4961.

(21) Garcia, R.; Perez, R. *Surf. Sci. Rep.* **2002**, *47*, 197.

(22) Stevens, R. M.; Nguyen, C. V.; Meyyappan, M. *IEEE Trans. Nanobiosci.* **2004**, *3*, 56.

(23) Yao, Z.; Postma, H. W. Ch.; Balents, L.; Dekker, C. *Nature* **1999**, *402*, 273.

(24) Tay, A. B. H.; Thong, J. T. L. *Rev. Sci. Instrum.* **2004**, *75*, 3248.